PREDICTION OF WEAR RATE OF TWO PEARLITIC RAIL STEELS USING A DYNARAT MODEL AND COMPARISONS TO FIELD TESTS AND TWIN–DISC EXPERIMENTS

F. A. Alwahdi[a], U. Olofsson[b], A. Kapoor[c] and F. J. Franklin[c]

[a]Department of Mechanical Engineering, The University of Omer Almukhtar,
P. O. Box 390 M Elbyada, Libya, E-mail: faragalwahdi@hotmail.com
[b]Department of Machine Design, Royal Institute of Technology,
KTH, SE, 10044 Stockholm, Sweden
[c]Department of Mechanical Engineering, The University of Sheffield,
Mappin Street, Sheffield, S1 3JD, UK

الملخص

تهدف الدراسة الحالية إلى اختبار مدى صلاحية نموذج دينارات (Dynarat model) باستخدام البيانات والملاحظات المستخلصة من تجارب حقلية على نوعين من قضبان السكك الحديدية، ومن تجارب معملية أجريت على آلة الأقراص المزدوجة. يعرض النموذج نتائج البري الناتجة من الانفعال المتراكم لمادة مطيلة معرضة لإجهاد متكرر نتيجة التلامس بالتدحرج أوالانزلاق أو الاثنين معاً.

أستخدم النموذج لمحاكاة التلامس بين القضيب الحديدي الخارجي وعجلة القطار عند المنحنيات حيث يتم التلامس بينهما عند رأس القضيب والحافة الداخلية له. تمت المحاكاة للانزلاق الكامل عند الحافة الداخلية للقضيب لمعامل احتكاك محدد وعلى النقيض تمت المحاكاة للانزلاق الجزئي عند رأس القضيب. تعرض الدراسة مقارنة بين نتائج نموذج المحاكاة والنتائج المتحصل عليها من التجارب الحقلية والمعملية، وتوصي بتطوير النموذج حتى يعطي نتائج أفضل.

ABSTRACT

The objective of this work is to validate the Dynarat model using data and observations of two rails in ordinary operation (field test) and twin disc experiments. The model successfully predicted the ratchetting wear of a ductile material subjected to repeated stress from rolling/sliding contact. Particular emphasis was placed on the work-hardening properties of the rail material. The wear modelling was used to simulate wheel-rail contact on the high rail in a curve, where there are contacts both on the top and at the gauge corner of the rail. The simulations were performed with full slip at the gauge corner of the rail with a given coefficient of friction. In contrast, at the rail head the simulations were performed with partial slip. Comparisons between simulated and measured wear, including field and laboratory tests, were presented. Further development of the model is needed.

KEYWORDS: Wear; Computer simulation; Ratchetting failure; Pearlitic rail steel; Field test.

INTRODUCTION

Wheel load is transmitted to the rail through a tiny contact area under high contact stresses. This results in repeated loading above the elastic limit which leads to plastic deformation. For contacts loaded beneath the elastic shakedown limit, shakedown occurs after a few load cycles and therefore the material deforms elastically [1]. For loads above the plastic shakedown limit, plastic ratchetting will occur, i.e. small increments of plastic deformation are accumulated with each pass of the wheel [2]. In rolling/sliding contacts, the amount of ratchetting is a function of the coefficient of traction (t_c) and the ratchetting starts after elastic behaviour without a plastic shakedown stage if t_c is greater than 0.25 the maximum contact pressure (p_0); the number of cycles (passes of the wheel); and the shear yield stress of the material (k). There are two ways in which ratchetting wear takes place in ductile materials. In the first, applicable in conditions of low load and where there is a low coefficient of friction, the material in a thin subsurface layer undergoes plastic ratchetting and is extruded out in the form of thin slivers which subsequently break off to providing wear debris. The mechanism of wear by extrusion has been modelled by Kapoor and Johnson [3,4]. The second model is applicable in conditions of high load and when there is a high coefficient of friction or where extrusion of slivers is not possible, such as in long discs. Extrusion of slivers from edges of the disc causes wear by plastic flow, whereas at the centre such extrusion is not possible and wear occurs by ratchetting failure. When the accumulated plastic strain at the contact surface (by ratchetting) reaches a critical value, the material fails and wear particles are formed. Kapoor and Franklin [5,6] developed a computer program, called Dynarat, which simulates the rolling/sliding contact of a cylinder, or wheel, with a ductile material. The material accumulates plastic shear strain when the orthogonal shear stress (the dominant stress following the build-up of residual stresses) exceeds the shear yield stress (which may increases if the material work-hardens). When the accumulated strain exceeds a critical value, the ductility is exhausted and the material is deemed to have failed. The model can estimate the ratchetting wear of a ductile material subjected to repeated stress from rolling/sliding contact. The ratchetting wear was computed using a ratchetting criterion proposed by Kapoor [4]. The model successfully predicted changes in wear rate from the beginning to the 'steady state', and could model strain hardening of the material with accumulation of deformation in the sub-surface material. The benefits of this computer simulation model, if validated, include:

- Wear rate for new rail material can be estimated to aid maintenance planning.
- Costly field measurements can be avoided. These types of analysis can be performed quickly and in a cost effective way by means of simulations, in contrast to lengthy and expensive field or laboratory measurements.
- The model is not a finite element model, which would be required for all material constraints to be met, but it has the benefit of computational speed. Thousands of stress cycles can be modelled in a matter of minutes.

Work hardening is introduced into the model through the effective shear yield stress (k_{eff}) which is related to the initial shear yield stress (k_0) and the total accumulated shear strain (γ) by a modified Voce equation [5].

$$k_{eff} = k_0 \max\{1, \beta\sqrt{1-\exp(-\alpha\gamma)}\} \quad (1)$$

The constants α and β are material parameters; α is a measure of how quickly the material hardens, and β is a measure of how much it hardens.

In wheel-rail contact, both rolling and sliding occur. On straight track, the wheel tread is in contact with the rail head, but in curves the wheel flange may be in contact with the gauge corner of the rail. Due to the conicity of the wheel profile, flanging results in a large sliding motion in the contact [7]. The specification of sliding is not so straightforward since some contact points at the interface may slip while others may stick. The influence of partial slip on wear rate has been examined by Franklin et al. [8] and Alwahdi et al. [9] using the Dynarat model. The purpose of this investigation is to validate the Dynarat model by comparing the predicated wear results with results of a field test and twin disc machine experiments of two pearlitic rail steels [10,11]. The model was used to simulate wheel-rail contact on the high rail in a curve, where there are contacts both on the top and gauge corner of the rail. The simulations were performed with full slip at the gauge corner of the rail with a given coefficient of friction. In contrast, at the rail head the simulations were performed with partial slip. A comparison between simulated and measured wear, including field test and twin-disc machine, is presented.

DETAILS OF THE FIELD TEST OF TWO PEARLITIC RAIL STEELS

Test sites

The Stockholm local network had been the subject of a national Swedish transport programme (the Stockholm test case) [10,12,13] in which the wear, surface cracks, plastic deformation and friction of rail and wheel had been observed for a period of two years. The data from the Stockholm test case has been used for validation of different wear models [11,14] and also surface crack models [15]. The model was employed for real traffic situations at the test sites. Four test sites were selected (A-D) because they contain two different types of pearlitic rail steel in the same curve [10]. These are located in Älvsjö on the Banverket track near Stockholm. The track carries, almost exclusively, unidirectional commuter trains travelling at an average speed of 75 km/h, but this varies slightly depending on the volume of traffic. The two types of vehicles used are:

- X1: motor coach (axle load 12 tons) plus trailing coach (axle load 7.5 tons), and
- X10: motor coach (axle load 15 tons) plus trailing coach (axle load 10.5 tons).

The test site is a curve with double tracks (see the schematic view of the Älvsjö test track in Figure 1). The outer track, Curve 1 (i.e. the track with a radius of 346 m), was lubricated with Terminus SSF 000 G. Two pearlitic rail steels were used: UIC 900A grade rail with ultimate stress 900 MPa and yield stress 507 MPa at site A, and UIC 1100 grade rail with ultimate stress 1100 MPa and yield stress 710 MPa at site B. The inner track, Curve 2 (i.e. the track with a radius of 303 m), has not been lubricated since March 1996, prior the test start in May 1997. Here again, UIC 900A grade and UIC 1100 grade rail were used. The track was rerailed with new rails in 1993 and ground in

1994. In May 1997 new test rails, each 20 m long, were inserted in the high rails of the two curves. Inserting new rails in the test track enabled initial wear on the newly inserted rail to be studied.

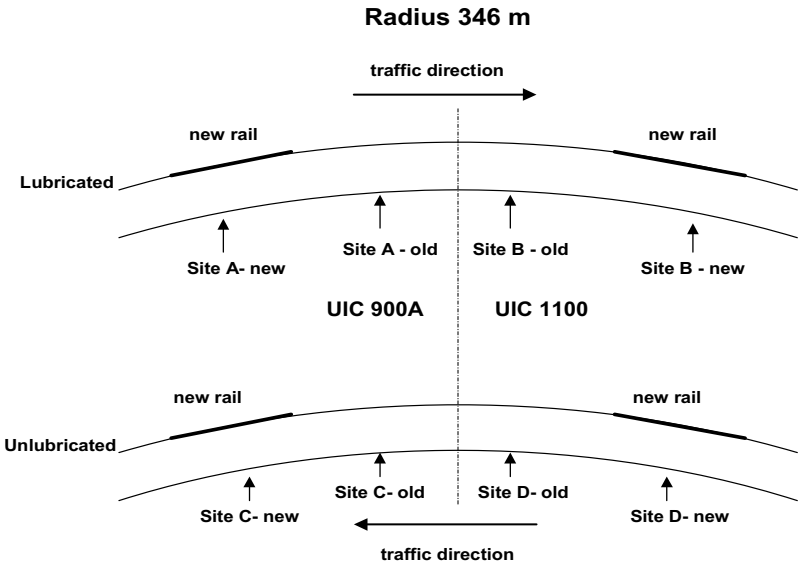

Figure 1: Schematic view of the Älvsjö test track [12].

The estimated number of cycles

Two types of vehicles were used, X1 and X10 trains, both operating in pairs with one powered unit and one trailing unit. Approximately two thirds of the commuter traffic is the X1 train. The axle load (motor and trailing coach) of the X1 train is approximately 19.5 tons without passengers. The axle load (motor and trailing coach) of the X10 train is approximately 25.5 tons without passengers. The average traffic axle load on each test curve was approximately 6 Mt per year. The total axle load after 16 months of traffic is 8.1 Mt.

$$\text{The average axle load of X1 and X10} = \frac{2}{3} \times 19.5 + \frac{1}{3} \times 25.5 = 21.5 \,\text{tons.}$$

$$\text{The total number of cycles after 16 months traffic} = \frac{8.1 \times 10^6}{21.5} = 376744 \,\text{cycles.}$$

Measurement results from the track

At the test sites measurements and observations of the rails were made several times during the project. Directly after the new test rails were inserted in the high rails of the two curves, the profiles and the hardness of the rail head and gauge corner were measured. The measurements were made from time to time during a 16 months period of traffic. Data on the coefficient of friction were produced with field instruments (Salient System Tribometer). The measuring principle is to measure the normal and the tangential forces between a test wheel and the rail when retarding the wheel from rolling

to complete sliding. The coefficient of friction is determined when the rotation of the wheel stops prior to the onset of slip. Measurements were performed on the rail head and on the rail edge of both the high and the low rail.

Profile measurements

The Miniprof system was used to measure the form of the rail. Further details on the profile system are described in Ref. [10]. For the low rail, the change was found to be too small to be accurately measured with the Miniprof system. Profiles were recorded using Miniprof at regular intervals, and three variables (W1, W2 and W3) were used in the quantitative comparison of wear rates for the rail. W1 is the vertical difference and is a measure of the wear on the rail head, which is often mild. W2 is the horizontal difference and W3 is the 45° difference. Both W2 and W3 are measures of wear at rail edge, which is often severe. The three variables are shown in Figure (2).

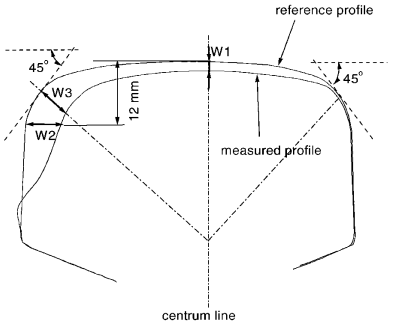

Figure 2: Schematic showing the three wear variables, [10].

TWIN DISC MACHINE TESTING

Olofsson and Telliskivi [11] performed a series of twin disc tests at the Tribology laboratory at the Otto von Guericke University of Magdeburg. The rig had two horizontal shafts having the same rate of revolution. The top discs were 32.5mm in radius, while the radii of the smaller bottom discs varied, depending on creepage required. The diameter ratios of the dissimilar discs represent 0.5% and 1.5% creepage. The wheel discs were produced such that they had a crowned surface, whereas the top of the rail discs was flat. The discs profiles were measured and the disc were weighed during the frequent interruptions of the tests in order to determine the characteristics of wear. The creepage, or amount of slip between the discs, can be calculated by:

$$\xi(\%) = 200\left(\frac{R_{Top}N_{Top} - R_{Bottom}N_{Bottom}}{R_{Top}N_{Top} + R_{Bottom}N_{Bottom}}\right) \quad (2)$$

where R is the radius of the disc specimen, N is the angular velocity of the disc, and the subscripts refer to the position of the discs on the machine. The creepage, or amount of slip between the discs when the angular velocities are equal, can be calculated by:

$$\xi(\%)=200\left(\frac{R_{Top}-R_{Bottom}}{R_{Top}+R_{Bottom}}\right) \quad (3)$$

In the analysis of the experiment, the coefficient of friction in rolling was given as:

$$\mu=\frac{0.5(M_{Top}+M_{Bottom})}{F_n 0.5(R_{Top}+R_{Bottom})} \quad (4)$$

where M_{Top} and M_{Bottom} are the torques (Nm) acting on the respective wheel and F_n is a normal load (N).

Wheel and rail test specimens were cut from wheel pieces from the rolling stock and rail sections that had been in use in the field test. The upper discs were machined from rail heads with their faces parallel to the base of the rail. The lower discs were machined from the outer section of the wheel with their faces parallel to the wheel radius. Prior to the test, the discs were cleaned in ethanol using an ultrasonic bath and their weight is recorded using an analytical balance so that wear loss during the test could be measured. The tests were carried out at room temperature. The total duration of the tests was 200000 revolutions. Two levels of loading and two levels of creepage were applied. The load was controlled by a coil spring whose normal force was approximately 300 N or 1600 N and a constant rotational speed of 300 rpm was used for both discs. All discs were sectioned, specimens were mounted, ground and polished before microhardness profiles below the contact surface were recorded.

RESULTS

Model validation by field test

Data and observations from a field test were compared with wear-rate results from computer simulations. The semi-contact width (a) is calculated from Equation (5) for each contact pressure, where R is the radius of the wheel (the wheel radius is R = 0.46 m for both X1 and X2 motor coaches), E^* is the elastic contact modulus and p_0 is the peak contact pressure.

$$a=\frac{2Rp_0}{E^*} \quad (5)$$

Elastic modulus and Poisson's ratio of both wheel and rail are 212GPa and 0.3 respectively. Elastic contact modulus (E^*) is therefore116.4 GPa. The critical shear strain (γ_c) is taken to have a mean of 8.8, the value estimated for UIC 900A grade rail steel, and a mean of 12 for UIC 1100 grade rail steel (with a standard deviation of 5% of the mean); these values are obtained from twin-disc tests [16-18]. Note that the total shear strain is measured by the tangent of the angle of plastic deformation (θ) in the twin disc test specimens. In this case θ is the angle of deformed structure measured at 0.2 mm below the contact surface. This method of shear strain measurement was used by Tyfour et al. [19] and was found to give a reasonably accurate measure of strain. For the purpose of modeling, both critical shear strain (γ_c) and the initial shear yield stress (k_0) have standard deviations of 5% of their means.

The train used in this study had been previously modelled with train dynamic simulation software such as GENSYS [20] and MEDYNA [21]. For the leading boggie, the first wheelset was in contact at the high rail gauge corner and the second wheelset was in contact at the high rail head. At the rail gauge corner contact, the tangential load reached its saturation value, and the entire contact was in a state of sliding. In contrast, at the rail head the contact was a rolling and sliding contact. A clear difference was found between the rail head wheel tread contact and the rail gauge-wheel flange contacts in terms of contact pressure. Peak Hertzian pressures (p_0) in the range 1.5-3.5 GPa have been chosen as previously modelled. It has been noted that due to a sharp radius, there is a pure sliding contact at the gauge corner-wheel flange contact (full slip model). In contrast, the rail head-wheel tread is a rolling/sliding contact in these tests and simulations with full-slip/ partial slip are performed.

Onset of wear in the Dynarat model is governed by the shear stress in the top layer of bricks. Initially the accumulated strain is zero everywhere, and the number of cycles required to accumulate the strain for failure depends critically on the shear stress and shear yield stress (which varies from brick to brick) in the top layer of bricks. For low coefficients of friction the maximum shear stress is subsurface and the stress in the surface layer of bricks is likely to be less than the shear yield stress so that there will be no accumulation of plastic shear strain at the surface and the top layer of bricks will never fail, and thus there will be no ratchetting wear at all (wear by other mechanisms will still exist, but is not modelled). Generally, the wear rate will be lower for the top layer of bricks and it will take a long time to fail. However, once the top layer of bricks fails, subsequent bricks will be close to the critical shear strain and will fail in quick succession, so that there is usually a prominent spike in the wear rate at that point. In cases of relatively high wear rate, the wear rate generally reaches a "steady state"; random variation of material properties will cause some fluctuation of the wear rate even in the steady state.

Figure (3) shows the results from a full slip simulation over 376744 cycles at the gauge corner of the new rail UIC 900A (Site A gauge corner). There is work hardening with α=75.2, β=2.22 (the ratio of the limiting hardness to the original hardness as it is measured on the field test).

The simulation is performed with different peak contact pressures p_0 =2.0, 2.25 and 2.70 GPa, and with a coefficient of friction μ = 0.32 (as it is measured on the field test), the mean yield stress (σ_y) is 507 MPa. There are two lines, corresponding to peak contact pressures p_0=2.25 GPa and p_0=2.70 GPa, of wear rate against number of cycles. The wear rate is zero for the third peak contact pressure (2.0 GPa).

There is an initial period (thousands of cycles) in which no wear rate occurs for all p_0 values. This is because the top layer starts with zero accumulated strain and many cycles must pass before the accumulated strain reaches the critical value for this layer of bricks to wear. The average wear rate predicted from the computer simulation for p_0=2.25GPa is $\Delta\omega$ = 1.29 nm/cycle (ω= 0.482 mm) and $\Delta\omega$ = 262 nm/cycle (ω = 98.56mm) for p_0=2.70GPa. Wear rate from the field test for the high rail after 16 months of traffic is W3 = 0.48 ± 0.10 mm and W2 = 0.57 ± 0.22 mm. It is interesting to note that the wear rate from the computer simulation at 2.25 GPa contact pressure is approximately equal to the wear rate from the field test.

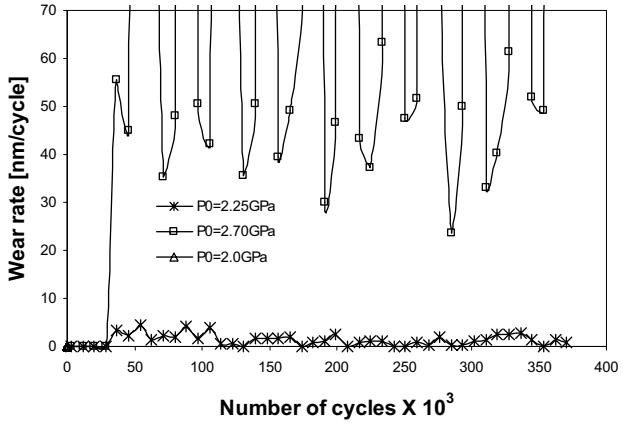

Figure 3: Evolution of wear rate with time for new rail UIC 900A (Site A gauge corner), μ =0.32, γ_c=8.8, σ_y=507MPa, p_0 =2.0, 2.25, 2.70 GPa and work hardening with α =75.2 and β =2.22.

Figure (4) shows the results from a simulation over 376744 cycles at the gauge corner of the old rail UIC 900A (Site A gauge corner). There is work hardening with α =62.38, β =2.36. The simulation is performed with different peak contact pressures p_0 =2.0, 2.25, 2.70 and 3.0 GPa, with a coefficient of friction μ = 0.25, and the mean yield stress σ_y = 507MPa.

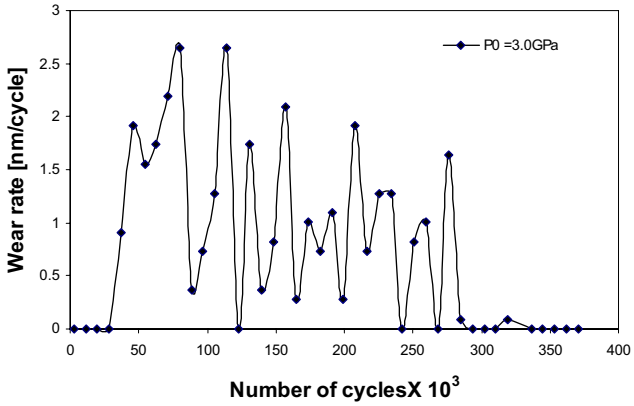

Figure 4: Evolution of wear rate with time for old rail UIC 900A (Site A gauge corner), μ =0.25, γ_c=8.8, σ_y=507MPa, p_0 =3.0GPa and work hardening with α =62.38 and β =2.36.

There is one line, corresponding to peak contact pressures p_0 = 3.0 GPa, of wear rate against number of cycles. The wear rate is zero (i.e., no wear rate) for other peak contact pressures. The average wear rate from the computer simulation for p_0=3.0GPa is $\Delta\omega$ =

0.77 nm/cycle (ω= 0.289 mm). The wear for the high rail gauge corner after 16 months of traffic was approximately W2 = 0.12 ± 0.03 mm and W3 = 0.04 ± 0.02 mm.

Comparison of the wear results

Comparison is made between the wear of the rail head as well as the gauge corner sides of high rail and the simulated wear after 16 months traffic of the two types of vehicles used, X1 and X10 trains. Four sites (Sites A-D) in two curves were selected for these comparisons. These contain two different types of pearlitic rail steel in each curve (UIC 900A grade rail and UIC 1100 grade rail). One of the curves was lubricated and the other one was dry. It is important to remember that lubrication is often applied only to the outer rail of the curve (at the gauge face of the high rail). Tables (1, 2, 3 and 4) summarize the comparison of the simulated wear results with the field test. The simulated wear given in a range depended on the applied pressures during the simulations. The peak pressure ranges have been chosen as previously modelled [20,21]. A clear difference was found between the rail head-wheel tread contact and the rail gauge-wheel flange contact in terms of contact pressure and sliding velocity. At the rail gauge corner contact, the tangential load reached its saturation value, and the entire contact was in a state of sliding. In contrast, at the rail head the contact was in a state of rolling and sliding contact. For the rail head-wheel tread contact, the simulations were performed under conditions of partial slip (with friction and traction coefficients values (t_c= 0.199)) and peak pressure did not exceed 2.50 GPa. In the rail gauge-wheel flange contact, the simulations were performed under conditions of full slip (with coefficient of friction values) and peak pressure was never above 3.50 GPa. The coefficient of frictions used in the simulation were similar to those measured in the field test. A significant difference in the coefficient of friction between the lubricated and the unlubricated test sites could be noted. The coefficient of friction has an important effect in the simulated wear. A lower coefficient of friction leads to a reduction of the value of the maximum orthogonal shear stress, and thus causes the shear strain increment per cycle to decrease. This increases the number of cycles to failure and as a result, the wear rate decreases. In this simulation, the friction and traction coefficients do not change with number of rolling cycles. Tyfour et al. [19] measured traction coefficients for unlubricated contact of rail and wheel steels using a twin disc machine. It was found that during an initial period the traction coefficient increases to reach its maximum value, and then decreases gradually to a constant rate. The parameter β is the ratio of the limiting hardness to the original hardness; and the parameter α is a measure of how quickly the material hardens. The value of the parameter β was calculated as the ratio of the maximum hardness (the value of the hardness measured after 16 months of traffic in the field test) to the original hardness of the pearlitic rail steel used in that test site. The value of the parameter α was calculated by using Voce equation (Equation (1)). The semi-contact width (a) was calculated from Equation (5) for each contact pressure, where the radius of the wheel was R = 0.46 m (the wheel radius for both X1 and X10 motor coaches). For the simulated wear, the wear rate was very sensitive to the change in the peak contact pressure. After a certain threshold of the peak contact pressure (when the pressure exceeds the shakedown limit), a small increase in the peak contact pressure causes very large increase in the wear rate.

Table 1: Comparison of the wear from field tests with computer simulation results for lubricated high pearlitic rail steel UIC 900A at curved track.

	Site A new rail			Site A old rail		
Wear parameters	W1	W2	W3	W1	W2	W3
p_0 (GPa)	1.50-2.25	2.0-2.70	2.0-2.70	1.50-2.25	2.0-3.0	2.0-3.0
μ	0.29±0.01	0.32±0.08	0.32±0.08	0.32±0.01	0.25±0.01	0.25±0.01
t_c	0.199	Full slip	Full slip	0.199	Full slip	Full slip
γ_c	8.8	8.8	8.8	8.8	8.8	8.8
Field test wear (mm)	0.08±0.01	0.57±0.22	0.48±0.10	0.04±0.01	0.12±0.03	0.04±0.02
Simulated wear (mm)	0-0.057	0-98.56	0-98.56	0-0.071	0-0.282	0-0.282
β, α	2.1, 85.7	2.22, 75.2	2.22, 75.2	2.24, 71.6	2.36, 62.4	2.36, 62.4
a (mm)	11.2-16.7	14.8-20.1	14.8-20.1	11.2-16.7	14.8-22.2	14.8-22.2

a is the semi-contact width

Table 2: Comparison of the wear from field tests with computer simulation results for lubricated high pearlitic rail steel UIC 1100 at curved track.

	Site B new rail			Site B old rail		
Wear parameters	W1	W2	W3	W1	W2	W3
p_0 (GPa)	1.5-2.25	2.0-2.7	2.0-2.7	1.5-2.5	2.0-2.7	2.0-2.7
μ	0.34±0.00	0.37±0.01	0.37±0.01	0.33±0.01	0.33±0.03	0.33±0.03
t_c	0.199	Full slip	Full slip	0.199	Full slip	Full slip
γ_c	12	12	12	12	12	12
Field test wear (mm)	0.06±0.05	0.14±0.10	0.14±0.04	0.06±0.02	0.24±0.04	0.08±0.04
Simulated wear (mm)	0 -0.015	0-57.54	0-57.54	0-0.071	0-5.89	0-5.89
β, α	1.7, 118.4	1.8, 100.6	1.8, 100.6	1.8, 104.3	1.88, 92.9	1.88, 92.9
a (mm)	11.2-16.7	14.8-20.1	14.8-20.1	11.2-18.5	14.8-20.1	14.8-20.1

a is the semi-contact width

Table 3: Comparison of the wear from field tests with computer simulation results for dry high pearlitic rail steel UIC 900A at curved track.

	Site C new rail			Site C old rail		
Wear parameters	W1	W2	W3	W1	W2	W3
p_0 (GPa)	1.5-2.0	2.25-3.50	2.25-3.50	1.5-2.0	2.0-2.7	2.0-2.7
μ	0.67±0.03	0.24±0.00	0.24±0.00	0.67±0.01	0.33±0.01	0.33±0.01
t_c	0.199	Full slip	Full slip	0.199	Full slip	Full slip
γ_c	8.8	8.8	8.8	8.8	8.8	8.8
Field test wear (mm)	0.38±0.11	4.07±0.11	3.29±0.09	0.12±0.05	1.89±0.13	1.29±0.14
Simulated wear mm)	0.08-9.89	0 – 4.16	0 – 4.16	0.02-4.57	0-35.23	0-35.23
β, α	2.26, 70.6	2.43, 57.9	2.43, 57.9	2.43, 57.9	2.47, 55.5	2.47, 55.5
a (mm)	11.2-14.8	16.7-25.9	16.7-25.9	11.2-14.8	14.8-20.1	14.8-20.1

a is the semi-contact width

Table 4: Comparison of the wear from field tests with computer simulation results for dry high pearlitic rail steel UIC 1100 at curved track.

	Site D new rail			Site D old rail		
Wear parameters	W1	W2	W3	W1	W2	W3
p_0 (GPa)	1.50-1.75	2.0-2.35	2.0-2.35	1.50-2.0	2.0-2.25	2.0-2.25
μ	0.66±0.01	0.39±0.02	0.39±0.02	0.60±0.01	0.47±0.03	0.47±0.03
t_c	0.199	Full slip	Full slip	0.199	Full slip	Full slip
γ_c	12	12	12	12	12	12
Field test wear (mm)	0.16±0.03	1.28±0.18	0.94±0.13	0.14±0.04	1.12±0.07	0.83±0.06
Simulated wear (mm)	0.01-0.36	0-1.33	0-1.33	0 – 0.139	1.11-13.8	1.11-13.8
β, α	1.76, 114	1.92, 87.4	1.92, 87.4	1.97, 81.2	1.97, 81.2	1.97, 81.2
a (mm)	11.2-12.9	14.8-17.4	14.8-17.4	11.1-14.8	14.8-16.7	14.8-16.7

a is the semi-contact width

Twin-disc experiment model validation

The simulation results were compared with the results of twin-disc experiments. Two levels of loading and two levels of creepage were applied. The traction coefficient is obtained using Carter's equation [22], Equation (6), assuming the coefficient of friction is constant:

$$t_c = -\mu\left[\left[\frac{\xi E^*}{2\mu p_0}+1\right]^2 - 1\right] \quad (6)$$

where μ is the coefficient of friction, E^* is the elastic contact modulus and ξ is the tangential creepage (slide/roll ratio). p_0 is the peak Hertzian pressure. The semi-contact width (a) is calculated from the Equation (5) for each contact pressure.

Table (5) summarizes the wear in twin-disc experiments and computer simulations. The simulations are performed over 200,000 cycles with a mean initial yield stress of σ_y= 507MPa. Two values of coefficient of friction (the maximum and the minimum values of coefficient of friction during each test) were used. The peak contact pressure were p_0 = 800MPa and 1400MPa, and there was an existing work hardening.

Table 5: Comparison of the wear from twin-disc machine experiment and computer simulation results for rail steel UIC 900 (dry testing).

Creepage (ξ%)	0.5		1.5	
F_n (N)	300	1600	300	1600
p_0 (MPa)	800	1400	800	1400
Semi-contact width (mm)	0.24	0.40	0.24	0.40
μ	0.417 - 0.638	0.538 - 0.562	0.729 - 0.752	0.556 - 0.60
t_c	0.41 - 0.52	0.33 - 0.42	0.55 - 0.60	0.55 - 0.60
γ_c	8.8	8.8	8.8	8.8
β, α	1.70, 176.94	1.95, 56.68	1.86, 125.14	2.0, 52.81
Simulated average wear rate (nm/cycle) †	0 - 0.066	0.039 - 0.571	0.282 - 0.528	0.320 - 2.914
Simulated total wear (μm) ‡	0 - 25	8 - 114	56 - 106	64 - 582
Experimental wear (μm)	7	22	12	25

† Simulated average wear rate is the mean wear rate for results of new, 500 cycles and 30000 cycles disc profile simulations.

‡Simulated total wear = simulated average wear rate × number of cycles

DISCUSSION

The major restriction of this model in the current form is its two-dimensional contact. Application of the Hertz theory (line contacts) leads to special difficulties not encountered in general three-dimensional contacts. In practice, the rail/wheel contact patch is approximately elliptic. Dynamic simulations predict a wide range of shapes and often wheel and rail make contact in two locations. The contact patch is of variable size and shape depending on the profile of the wheel and rail. Also the displacement of the wheelset away from the centreline of the track causes variation of contact patch shape and can produce multiple points of contact including flange contact. Extending the model to a full three-dimensional contact stress distribution is possible. Wear rate is expected to drop for a given peak pressure, since stresses decay faster with depth than for two-dimensional contact used in the above model [8]. In the current model, the surface roughness is not taken into account (contact assumed smooth). Surface roughness greatly influences contact pressure, as stated by Seabra and Berthe [23]. Numerical analysis showed that roughness causes the contact pressure to deviate from

the assumed Hertzian to one with very high sharp peaks. Work by Kapoor et al. [24] on conformal contacts showed that, even at low loads, surface roughness plays an important role in subjecting a thin layer to severe contact stresses. Contact pressures at asperities were found to be much higher than the average nominal pressure. Even under normal operating conditions and with smooth surface finishes, these pressures can exceed the shakedown limit. In practice, surfaces are rough and the corresponding pressure distributions arising at the contacts between surfaces are much more complex. The surfaces make contact over a number of small areas within the contact region, and the pressures at these asperities are far higher than the pressure predicted for smooth contact. One consequence of this is that the subsurface stress distribution predicated for smooth contact is altered significantly. The removal of bricks causes surface roughness, and this would result in very high pressures at asperity peaks and so the stresses experienced by bricks in the top layers would be far higher than for smooth contact.

The criterion for failure of the bricks used in the simulation was [5]:

$$\frac{\sum \gamma}{\gamma_c} \geq 1 \tag{7}$$

Once the accumulated plastic shear strain (γ) exceeds the critical shear strain for failure (γ_c), the material is supposed to have failed. In practice, it is possible that the material fails either by low cycle fatigue or by ratchetting failure. Kapoor [4] showed that the two failure mechanisms are independent and competitive and that the material fails by whichever is satisfied in the shorter number of cycles. The simulations only consider the ratchetting failure mechanism in which failure thus occurs when accumulated plastic shear strain of material reaches its critical shear strain.

Finally, to simplify the model, the simulation did not consider crack initiation or propagation in this study. However, ratchetting can be responsible for both the existence and early growth of cracks. Fletcher et al. [25] used results from the Dynarat ratchetting model developed to allow the simultaneous investigation of wear, crack initiation and early crack propagation, to identify small crack-like flaws. Image analysis was applied to the visual representation of the worn surface generated by the model. An image processing technique was developed to identify cracks within the output of the model. Plots from the model showed a good similarity to traditional micrographs taken from sections of worn surfaces. This enables both wear and early stages of rolling contact fatigue crack development to be studied simultaneously using a ratchetting-based model. Crack growth is dependent on the wear rate because cracks are defined to lie in material which has failed but not yet been removed. Wear and crack growth can therefore interact, with wear at the surface of a component leading to the truncation of existing surface breaking cracks.

CONCLUSIONS

A ratchetting wear computer model was developed at the University of Sheffield. The model is capable of successfully predicting the ratchetting wear of a ductile material subjected to repeated loading. The simulations were performed with the assumption of full slip at the gauge corner of the rail with a given coefficient of friction.

In contrast, at the rail head the simulations were performed with partial slip. The results from both sets of simulations and the field test showed difference in wear rate between rail head and the gauge corner side of the high rail. Comparisons have been made between simulated and measured high rail wear after 16 months of traffic. The measured wear at the test site is great lower of the wear predicted by the model for same operation conditions. The uncertainty in the predicted wear rate is too great to use the current Dynarat model as a reliable predictive tool. Another comparisons have been made between simulated and experimental wear after 200000 cycles for two different types of pearlitic rail steels tested. Further development of the model is needed, such as better representation of microstructural behaviour. In addition to that, the ratchetting equation, which drives the Dynarat model, needs to be improved to cover other rail materials and more loading configurations.

REFERNCES

[1] A. F. Bower, K. L. Johnson, Plastic flow and shakedown of the rail surface in repeated wheel-rail contact, Wear, 144 (1991) 1-18.

[2] A. Kapoor, K. L. Johnson, Plastic atcheting as a mechanism of metallic Wear, Proc. R. Soc. London 445 (1994) 367-381.

[3] A. Kapoor, K. L. Johnson, J. A. Williams, A model for the mild atcheting wear of metals, Wear, 200 (1996) 38-44.

[4] A. Kapoor, A re-evaluation of the life to rupture of ductile metals by cyclic plastic strain, Fatig. Fract. Enging. Mater. Struct., 17 (2) (1994) 201-219.

[5] A. Kapoor, F. J. Franklin, Tribological layers and wear of ductile materials, Wear, 245 (2000) 204-215.

[6] F. J. Franklin, I. Widiyarta, A. Kapoor, Computer simulation of wear and rolling contact fatigue, Wear, 251 (2001) 949-955.

[7] U. Olofsson, S. Andersson and S. Bjorklund, Simulation of mild wear in boundary lubricated spherical roller thrust bearing, Wear, 241 (2000) 180-185.

[8] F. J. Franklin, T. Chung and A. Kapoor, Ratchetting and fatigue-led wear in rail-wheel contact, Fatig. fract. enging. mater. struct., 26 (2003) 949-955.

[9] F. Alwahdi, F. J. Franklin and A. Kapoor, The effect of partial slip on the wear rate of rails, Wear, 258 (2005) 1031-1037.

[10] U. Olofsson and T. Telliskivi, Wear plastic deformation and friction of two rail steels-a field test and a laboratory study, Wear, 254 (2003) 80-93.

[11] T. Telliskivi, Wheel-rail interaction analysis, Ph.D. Thesis, Royal Institute of Technology, KTH, SE, Stockholm 2003.

[12] U. Olofsson, R. Nilsson, Surface cracks and wear of rail: a full scale test and laboratory study, Journal of Rail and Rapid Transit, vol. 216 (2002) 249-264.

[13] R. Nilsson, Wheel/Rail wear and surface cracks, Licentiate Thesis, KTH, Stockholm 2003.

[14] T. Jendel, Prediction of wheel profile wear – methodology and verification. Licentiate thesis, KTH, Vehicle Engineering, Sweden, 2000.

[15] J. Ringsberg, Rolling contact fatigue of railway rails with emphasis on crack initiation, Doctoral Thesis, Chalmers University of Technology, Göteborg (2000).

[16] D. F. Cannon, The fight against rail rolling contact fatigue, Int. Railway J. and Rapid Transit Rev. XXXIX(12) (1999) 27-28.

[17] D. F. Cannon, ICON partners. Int. Railway J. and Rapid Transit Rev. XL(2) (2000) 3-9.
[18] D. F. Cannon, Integrated study of rolling contact fatigue (ICON), final technical report, May 2000.
[19] W. R. Tyfour, J. H. Beynon and A. Kapoor, Deterioration of rolling contact fatigue life of pearlitic rail steel due to dry-wet rolling-sliding line contact, Wear, 197 (1996) 255-265.
[20] T. Jendel, Prediction of wheel profile wear-comparison with field measurements, Wear, 253 (2002) 89-99.
[21] K. Knothe, A. Theiler and S. Guney, Investigation of contact stresses on the wheel/rail-system at steady state curving, In Proceedings of the 16th IAVSD Conference on The Dynamics of Vehicles on Roads and on Tracks, Pretoria, South Africa, 30 August - 3 September 1999, Vol. 33, 616-628.
[22] F. W. Carter, On the action of a locomotive driving wheel, Proc. Roy. Soc., Series A112 (1926) 151-157.
[23] J. Seabra, D. Berthe, Influence of surface waviness and roughness on the normal pressure distribution in Hertzian contact, Trans. ASME, J. Tribology109 (1987) 462-470.
[24] A. Kapoor, F. J. Franklin, S. K. Wong and M. Ishida, Surface roughness and plastic flow in rail wheel contact, Wear, 253 (2002) 257-264.
[25] D. I. Fletcher, F. J. Franklin and A. Kapoor, Image analysis to reveal crack development using a computer simulation of wear and rolling contact fatigue, Fatig. fract. engng. mater. struct., 26 (2003) 957-967.